Alkaline Phosphatase Functionalized nanoparticles: Attachment, Enzyme Kinetics and Colloidal Diffusion

A Master's thesis by ©Anas Alhasanat submitted to the School of Graduate Studies in partial fulfillment of the requirements for the degree of

Master of Science

Department of Physics and Physical Oceanography
Memorial University of Newfoundland

March 2023

St John's Newfoundland and Labrador

Acknowledgments

I would like to express my sincere gratitude to my supervisor, Dr. Anand Yethiraj, for his invaluable guidance, support, and mentorship throughout this research. Dr. Yethiraj's expertise and insightful feedback were instrumental in shaping the direction of this study and ensuring its success. I am also grateful to Dr. Yethiraj for allowing me to work in the Soft Matter Group and serving as a role model and inspiration.

I thank Dr. Valerie Booth for her help with enzyme kinetics measurements and for using her lab to study colloidal diffusion. Her expertise in this area was invaluable to the success of this research. I am also grateful to Dr. Yuming Zhao for allowing us to use his lab to measure enzyme kinetics. His generosity and support were greatly appreciated and contributed to the success of this study. Additionally, I would like to thank Dr. Francesco Piazza and Dr. Hamacek Josef for their help with the enzyme kinetics study and analysis.

In addition, I want to thank everyone in the Soft Matter Group for their cooperation, support, and inspiration throughout this project. The effectiveness of this study was greatly influenced by insightful conversations, suggestions, and comments from the group members. I'm glad to be a member of a research community that is so encouraging and cooperative.

Last but not least, I would want to thank my family from the bottom of my heart for their unfailing support and inspiration throughout this research adventure. Their compassion and empathy have served as a constant source of inspiration and drive.

This research was supported by funding from the Natural Sciences and Engineering Research Council of Canada (NSERC), and I would like to express my appreciation for their support.

Abstract

Enzymes are proteins found in organisms that work as biological catalysts. In the last decade, some studies report that enzymes diffuse faster during catalysis [1], and recently others show the possibility of making enzyme-powered micromotors; where urease-functionalized microparticles appear to diffuse faster during catalysis as observed by trajectory tracking [2]. We studied the validity of using the enzyme alkaline phosphatase as a nanomotor on spherical polystyrene particles with a diameter of 200 nm (attached by glutaraldehyde coupling) using differential dynamic microscopy (DDM) and dynamic light scattering (DLS) to obtain the diffusion coefficient of those particles compared to bare particles of the same size looking for any enhanced particles motion. We will report on the existence (or absence) of enhancement in diffusivity. The enzyme activity of our alkaline phosphatase functionalized nanoparticles, obtained by spectroscopy and the Michaelis-Menten relation [3], was found to be very similar (slightly lower) to the bare alkaline phosphatase activity. DDM is a technique that exploits optical microscopy to obtain local quantitative information about dynamic samples (diffusion coefficient, particle size) by probing wave vector-dependent dynamics [4]. DDM could be used to study the dynamics in liquid suspensions, soft materials, cells, and tissues. In DDM, image sequences are analyzed via a combination of image differences and spatial Fourier transforms to obtain information equivalent to that obtained by means of dynamic light scattering (DLS) techniques. Compared to DLS and particle trajectory tracking, DDM offers obvious advantages, most importantly, providing high statistics by capturing a large number of particles, removing the static contributions along the optical path, flexibility of choosing an analysis region, and the power of simultaneous different microscopy contrast mechanisms. But those advantages come with a price; it is challenging to know the suitable settings (camera speed, objective magnification, sample dilution, etc.) for each measurement (i.e., each particle size). In order to validate our DDM setup, we studied a range of polystyrene particles size (60 nm-1 micron) suspended in water using different settings to conclude the suitable settings for each size in that range. Using previously published Python code [5] and modified by our group, we managed to analyze thousands of frames (images) with the speed of hundreds of frames per second for each measurement. All measurements were compared to DLS measurements on the same samples (but more diluted) for comparison.

Contents

List of Figures

List of Tables

Chapter 1

Introduction

1.1 Brownian Motion

The random motion of particles suspended in a medium, named after the botanist Robert Brown, who first described the phenomenon in 1827 while looking through a microscope at the pollen of the plant Clarkia Pulchella immersed in water [9]. In 1905, Albert Einstein published a paper where he modelled the motion of the pollen particles as being moved by individual water molecules, making one of his first major scientific contributions [10]. For spherical particles, by applying Stokes' law, the Brownian motion is described by the Stokes-Einstein relation:

$$D = \frac{k_B T}{3\pi\eta d}, \tag{1.1}$$

where $k_B T$ is the thermal energy (k_B being the Boltzmann constant and T the absolute temperature), η is the solvent viscosity, and d is the hydrodynamic diameter of the particles.

1.2 Dynamic Light Scattering (DLS)

The DLS technique has gained popularity as a simple, easy, and reproducible tool to measure the diffusion coefficient of nanoparticles in a dispersion, and hence the particle size using the Stokes-Einstein relation 1.1. Particles in a colloidal dispersion scatter light from an incident laser beam. The continuous Brownian motion of the particles within a dispersion causes constructive and destructive interferences; hence, scattered light intensity fluctuates over time [11]. This time-dependent intensity of the scattered light is detected in DLS. (see Figure 1.1A).

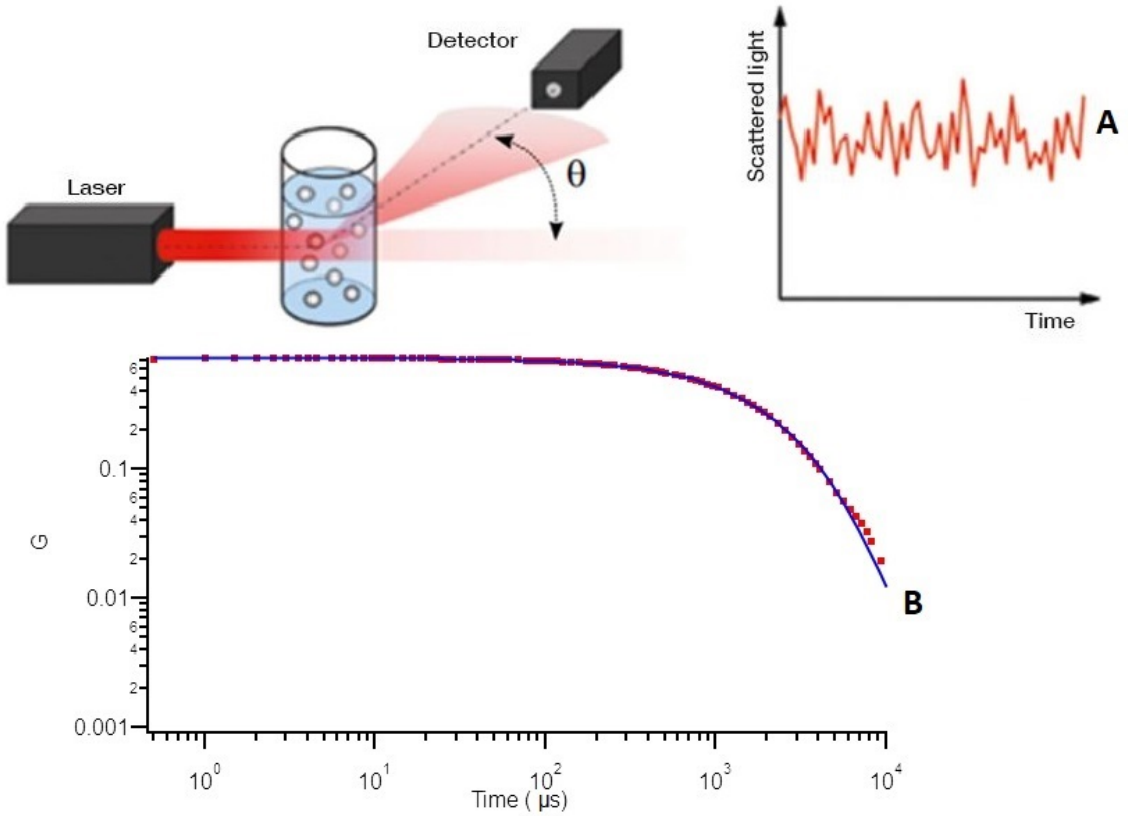

Figure 1.1: (A) Fluctuation in the intensity of the scattered light by the particles during DLS due to constructive and destructive interferences. (B) The correlogram for 1 μm diameter polystyrene particles dispersed in water.

In DLS, the fluctuation of intensity in scattered light is self correlated against time t. Figure 1.1B shows the intensity auto-correlation function $G(t) = \langle I(t_0)I(t_0+t)\rangle$, which has the functional dependence [12]:

$$G(t) = b + f\exp(-2Dq^2t), \tag{1.2}$$

where f is a constant dependent on the instrument and the optical settings, D is the diffusion coefficient, and q is the scattering vector which can further be expressed as

$$q = \frac{4\pi n\sin(\theta/2)}{\lambda}. \tag{1.3}$$

Here, n is the refractive index of the solvent, λ is the wavelength in vacuum, and θ is the scattering angle.

1.3 Differential Dynamic Microscopy (DDM)

DDM is a technique that exploits optical microscopy to obtain local quantitative information about a dynamic sample (diffusion coefficient, particles' size) by probing wave vector dependent dynamics. It can be used to study the dynamics in liquid suspensions, soft materials, cells, and tissues. In DDM, image sequences are analyzed via a combination of images' differences and spatial Fourier transforms to

obtain information equivalent to that obtained by means of light scattering (DLS) techniques. Compared to DLS, DDM offers obvious advantages. First, taking images' differences removes the static contributions along the optical path. Second, due to the microscopy technique, there is flexibility in choosing an analysis region, and one has access to different microscopy contrast mechanisms.

In 2008, Cerbino, Roberto, and Trappe [4] demonstrated the use of an ordinary white-light microscope for the study of the q-dependent dynamics of colloidal dispersions. They acquired a time series of digital video images in a bright field with a fast camera, and the images' differences were Fourier analyzed as a function of the time delay between them. This allowed for the characterization of particles' diffusion coefficients. The resulting diffusion coefficients were found to be in good agreement with the theoretically expected values for Brownian motion in a viscous medium using the Stokes-Einstein relation and the known particles' sizes.

By subtracting two images' intensities as a function of position and time separated by a time delay Δt, we have a time-delay-dependent signal $S(\Delta t)$ due to intensity fluctuation as the particles are undergoing Brownian motion,

$$S(\Delta t) = I(x, y; \Delta t) - I(x, y, 0). \tag{1.4}$$

Quantitative information about the system's dynamics from the images' differences can be obtained in two steps. The first step is to calculate the signal from Equation 1.4 in 2D Fourier space as:

$$F_S = \int S(x, y; \Delta t) exp[-i2\pi(u_x x + u_y y)] dxdy, \tag{1.5}$$

Now, using the Parseval theorem [13],

$$\int |F_S(u_x, u_y; \Delta t)|^2 du_x du_y = \int |S(x, y; \Delta t)|^2 dxdy = \sigma^2(\Delta t), \tag{1.6}$$

where $\sigma^2(\Delta t)$ is the spatial variance in real space. Equation 1.6 shows that the total energy content of S in real space is the same as F_S in Fourier space.

Secondly, using Equation 1.3, the Fourier components are associated with the scattering angle θ (hence the scattering vector q). The object imaged on the camera sensor is a superposition of different Fourier components characterized by a spatial frequency u_{obj} [13, 14]. Each frequency component diffracts light at angle $\theta = sin^{-1}(\lambda u_{obj})$ to the microscope's optical axis. A sinusoidal fringe pattern will be formed on the camera sensor due to the diffracted plane wave. This pattern, characterized by a spatial frequency $u_{det} = sin(\theta/\lambda)$, demonstrates the association between the spatial frequency on the detector u_{det} and the scattering angle θ.

For square images, with $N \times N$ pixels, it is possible to apply the fast Fourier transform (FFT) [15] to the images' difference. This allows to treat the one dimensional power spectrum $|F_S(u; \Delta t)|^2$, where $u = \sqrt{u_x^2 + u_y^2}$. For comparison with DLS, one obtains $|F_S(q; \Delta t)|^2$, where $q = 2\pi u$. $|F_S(q; \Delta t)|^2$ is found to increase with

Δt until saturates at longer time delays. The plateau value shifts to smaller Δt as the wave vector q increases, denoting a q dependence in the characteristic time of the system. For a quantitative description of this behaviour, the fluctuations in the intensity of the original images have been considered as concentration fluctuations in the sample [4]. For Brownian diffusion, the Fourier concentration mode has the following exponential time [16],

$$|F_S(q;\Delta t)|^2 \propto 1 - \exp(-\Delta t/\tau(q)), \tag{1.7}$$

where $\tau(q)$ is the characteristic time,

$$\tau(q) = 1/Dq^2. \tag{1.8}$$

DDM stands out among other techniques, like particle tracking, due to its ability to utilize every pixel on the camera as an individual sensor. This unique feature allows for high statistical accuracy and minimizes measurement errors when measuring the diffusion coefficient of spherical particles.

1.4 Enzyme Kinetics

Enzyme kinetics studies deal with time-dependent enzyme-catalyzed chemical reactions that tend to reach the equilibrium state. The study of enzyme kinetics is valuable in order to understand the mechanisms of enzyme catalysis and regulation. An enzyme is typically a protein molecule that catalyzes a reaction of another molecule (substrate). The substrate molecules bind to the "active site" of the enzyme to produce an enzyme-substrate complex and from there to product and enzyme, via a transition phase as shown in the mechanism [17, 18]:

$$\mathrm{S} + \mathrm{E} \rightleftharpoons \mathrm{ES} \rightleftharpoons \mathrm{P} + \mathrm{E}. \tag{1.9}$$

Enzyme kinetic studies start by observing the concentration of the substrate and its conversion into the product. But, since the enzyme catalyzed reactions involve a reaction of two reactants into a transition phase (the enzyme-substrate complex) and then into a product, it is useful to discuss **the chemical reaction order** [6]. A first-order reaction is the conversion of only one reactant A into a product P, which is considered the simplest chemical reaction:

$$\mathrm{A} \xrightarrow{\mathrm{k}} \mathrm{P}, \tag{1.10}$$

the reaction rate v can be determined from the time-dependent decrease in A or from the increase in P and is directly proportional to the amount of A:

$$v = -\frac{d[A]}{dt} = \frac{d[P]}{dt} = k[A]; \tag{1.11}$$

where, k is the first-order reaction rate constant, in the dimension of s^{-1}, independent of the concentration. A second-order reaction is the reaction of two reactants

with each other to form a product or more than one product (since the reaction is only in the forward direction):

$$\mathrm{A} + \mathrm{B} \xrightarrow{\mathrm{k}} \mathrm{P}. \tag{1.12}$$

In this case, the reaction rate v is proportional to the decrease in both A and B or the increase in P; hence,

$$v = -\frac{d[A]}{dt} = -\frac{d[B]}{dt} = \frac{d[P]}{dt} = k[A][B]. \tag{1.13}$$

The second-order reaction rate constant k ($\mathrm{s}^{-1}\mathrm{M}^{-1}$) includes a concentration term in its unit. The zero-order reaction is the most relevant reaction order to the enzyme mechanism; if a reaction is being catalyzed by a catalyst (such as an enzyme), as long as this catalyst is present in a very small amount, the reaction rate v will be independent of any reactant concentration. The following reaction describes the conversion of a substrate S into the product P catalyzed by a catalyst E, assuming the catalyst concentration is very small:

$$\mathrm{S} + \mathrm{E} \xrightarrow{\mathrm{k}} \mathrm{P} + \mathrm{E}. \tag{1.14}$$

Here, the reaction rate is independent of the substrate concentration,

$$v = -\frac{d[S]}{dt} = \frac{d[P]}{dt} = k. \tag{1.15}$$

1.4.1 The Steady State Assumption of Enzyme Kinetics

Victor Henri in 1902 [19], presented a primary equation describing the reaction catalyzed by the enzyme invertase. Leonor Michaelis and his Canadian coworker Maud Leonora Menten in 1913 [3], studied the validity of Henri's equation with the enzyme invertase. George Edward Briggs and John Burton Sanderson Haldane derived the Michaelis-Menten equation using the steady state assumption in 1925 [20], an equation describes the irreversible enzyme reaction that converts a single substrate into a product:

$$\mathrm{S} + \mathrm{E} \underset{\mathrm{k_{-1}}}{\overset{\mathrm{k_1}}{\rightleftharpoons}} \mathrm{ES} \xrightarrow{\mathrm{k_2}} \mathrm{P} + \mathrm{E}. \tag{1.16}$$

The substrate and the product variations over time are

$$\frac{d[S]}{dt} = -k_1[S][E] + k_{-1}[ES], \text{ and} \tag{1.17}$$

$$\frac{d[P]}{dt} = k_2[ES] = v. \tag{1.18}$$

The enzyme itself can either be free or associated with the enzyme-substrate complex. The concentrations of free enzyme and enzyme-substrate complex are

$$\frac{d[E]}{dt} = -k_1[S][E] + k_{-1}[ES] + k_2[ES], \text{ and} \tag{1.19}$$

$$\frac{d[ES]}{dt} = k_1[S][E] - k_{-1}[ES] - k_2[ES]. \tag{1.20}$$

The production of P is directly proportional to the enzyme-substrate complex ES, whereas the concentration of the enzyme-substrate complex depends on the concentration of P and E. But, it is difficult to calculate the time-dependent variations of the reactants. Here, the steady state assumption comes in handy, because it assumes constant concentrations of both the enzyme and the enzyme-substrate complex. The reaction undergoes three phases: a fast formation of the enzyme-substrate complex phase (pre-steady-state), the steady-state phase which has nearly constant enzyme-substrate complex concentration, and the substrate depletion phase where the enzyme-substrate complex decays.

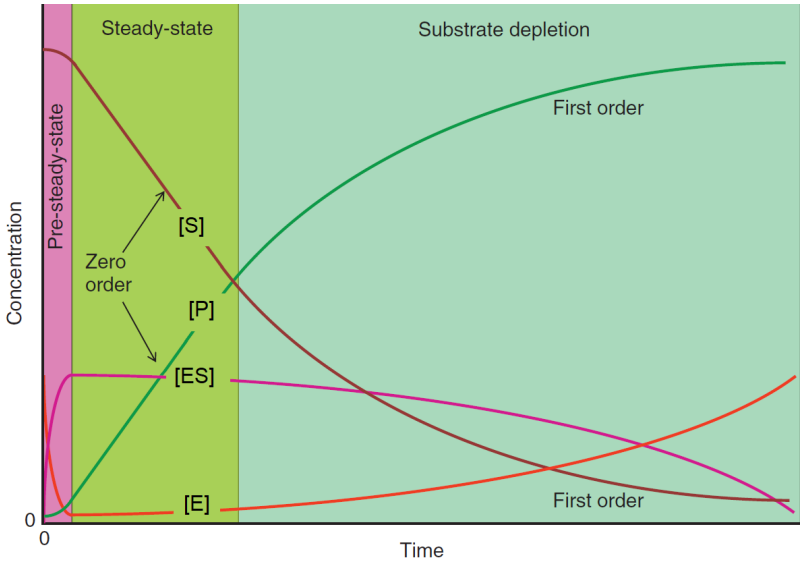

Figure 1.2: The changes of the reactant concentration versus time at each phase of an irreversible enzyme-catalyzed reaction. Reproduced with permission from [6].

Since the formation and the decay of enzyme-substrate complex are balanced during the steady state phase which is considerably long, both enzyme and enzyme-substrate complex amounts remain constants, equations 1.19 and 1.20 both reduce to

$$k_1[S][E] = (k_{-1} + k_2)[ES]. \tag{1.21}$$

The total enzyme concentration $[E]_0 = [E] + [ES]$ is taken to substitute [E],

$$[ES] = \frac{k_1[S][E]_0}{k_{-1} + k_2 + k_1[S]}. \tag{1.22}$$

By substituting $[ES]$ in equation 1.18, the Michaelis–Menten equation, a relation between the reaction rate and the substrate concentration, is obtained to be

$$v = \frac{V_{max}[S]}{K_m + [S]}. \tag{1.23}$$

In equation 1.23, the Michaelis–Menten constant $K_m = (k_{-1} + k_2)/k_1$, in molarity unit (M), is an inverse measure of enzyme affinity for its substrate. Another constant

used in Michaelis–Menten equation is $V_{max} = k_2[E]_0$ which is the maximum reaction achieved when all the available enzyme molecules participate in the reaction.

By taking the reciprocal of both sides of the Michaelis-Menten equation 1.23 and rearranging the terms, the Lineweaver–Burk equation described by Hans Lineweaver and Dean Burk in 1934 [21] transforms the hyperbolic curve into a straight line on a double-reciprocal plot.

$$v^{-1} = \frac{K_m}{V_{max}[S]} + V_{max}^{-1}. \tag{1.24}$$

1.4.2 Alkaline Phosphatase Kinetics by UV-Vis Spectroscopy

The enzyme alkaline phosphatase is found across a multitude of organisms. It dephosphorylates the non-specific substrate, p-nitrophenylphosphate (pNPP) in order to produce p-nitrophenol(pNP) and inorganic phosphate following the reaction shown in Figure 1.3.

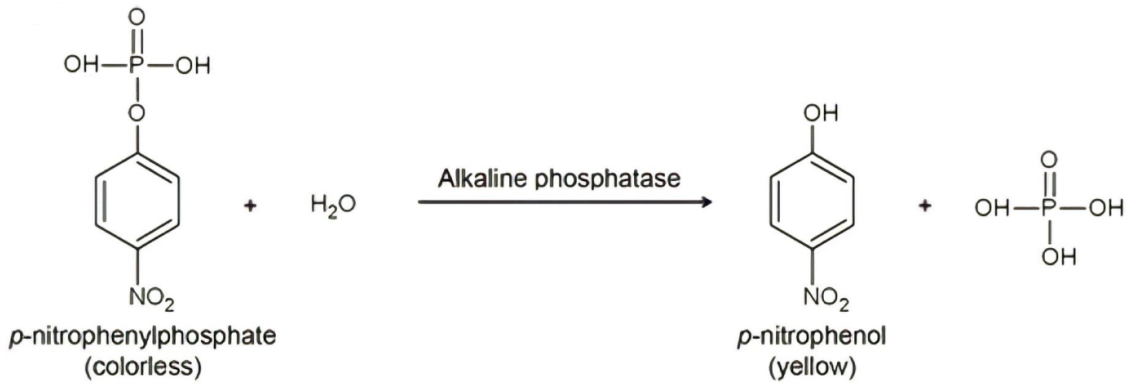

Figure 1.3: The production of p-nitrophenol (pNP) from p-nitrophenyl phosphate (pNPP) catalyzed by the enzyme alkaline phosphatase.

The conversion of the colourless substrate into a yellow product with an absorbance peak at $\lambda_{max} = 400$nm, see Figure 1.4, is a perfect reaction to use spectroscopy in order to study the reaction rate and alkaline phosphatase activity.

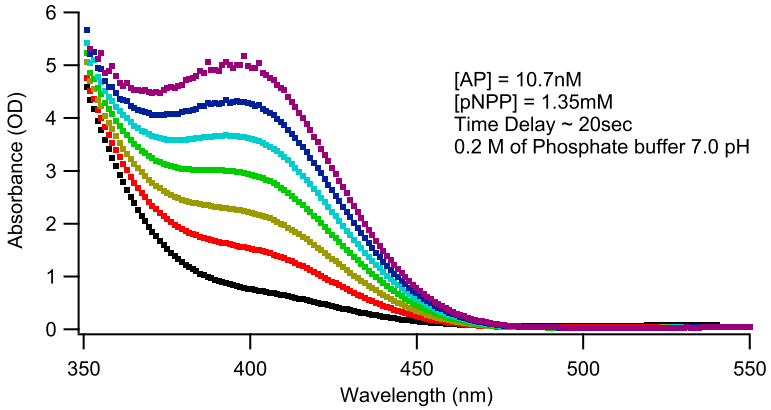

Figure 1.4: The increase of pNP over time in the presence of the alkaline phosphatase and its substrate pNPP in 0.2 M of phosphate buffer at 7.0 pH at 25 °C (the black-symbol spectrum being the earliest at $t = 0.25$ s, then red, yellow, etc., and finally purple at $t = 2.25$ s).

In Figure 1.4, the absorbance of 3 ml of the sample was measured using the Cary 6000i UV-Vis Spectrometer, in a wavelength range from 350 nm to 550 nm, and a scan rate of 1818 nm/min. Here, the black spectrum is the earliest at t = 0.25 s, then red, yellow, etc., and finally purple at $t = 2.25$ s. At wavelengths greater than 470 nm, there is no absorbance observed at any time. Conversely, at wavelengths smaller than 400 nm, absorbance increases over time and reaches a maximum at 400 nm. This supports the formation of the yellow-coloured product PNP.

By plotting the absorbance at the peak λ_{max} against time, the reaction rate v is obtained from the slop of the initial linear increase: see Figure 1.5. Repeating the reaction rate measurements for different known substrate (pNPP) concentrations at a fixed enzyme (alkaline phosphatase) concentration, and using Michaelis–Menten equation 1.23, the alkaline phosphatase kinetics constants were obtained: this is the subject of the next section.

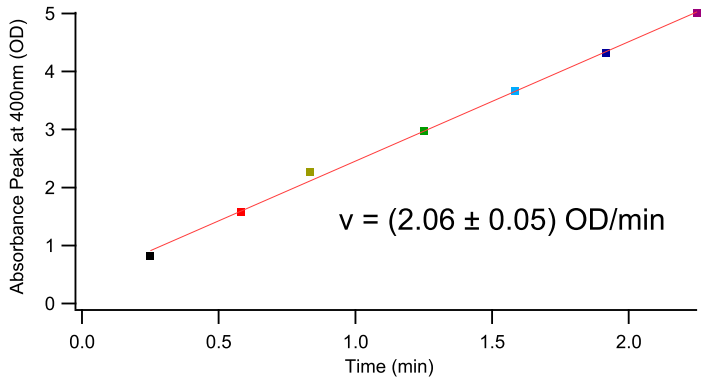

Figure 1.5: The absorbance peak at 400 nm from Figure 1.4, plotted against, time yields the reaction rate v.

1.5 Enzyme diffusion and nanomotors

The enhanced Diffusion of enzymes is a phenomenon that has been reported in a series of studies over the past two decades. Researchers have used a variety of techniques such as fluorescence correlation spectroscopy (FCS), far-field super-resolution stimulated-emission-depletion microscopy with FCS (STED-FCS), and DLS to measure the diffusion rates of enzymes and have observed apparent enhancements in the diffusion of a wide selection of enzymes. However, it has been suggested that some of these measurements may be influenced by fluorescence-related artifacts.

Two studies in 2009 [22, 23], reported that energy (or momentum) arising from catalytic reactions could drive the movement of particles on the micron and submicron size scales by self-electrophoresis, self-diffusiophoresis, and bubble propulsion. A year later, Muddana et al. [1], demonstrated the catalysis-induced increase of diffusion coefficient by 28% for the enzyme urease exposed to its substrate (urea) using fluorescence correlation microscopy (FCS). When urease was inhibited by pyrocatechol and exposed to urea again, the diffusion coefficient was significantly lower, supporting the idea of the catalysis-induced increase of diffusion coefficient. Sengupta [24], also reported enhanced diffusion using catalase, again using the FCS technique. Another study by Riedel et al. [25], reported enhanced diffusion measured via FCS in four enzymes: alkaline phosphatase, urease, catalase, and triose phosphatase isomerase. However, it should be noted that enzyme reactions that generate gases have an independent potential mode for propulsion, so the enhanced diffusion in catalase enzyme is probably real but should be disregarded in this discussion. Illien et al. [26], also reported enhanced diffusion in aldolase, indicating that if the enhancement is real, it occurs even when the reaction is endothermic. An earlier study in 1998, by Borsch et al. [27], also reported enhanced diffusion using FCS and F1-ATPase.

However, Gunther et al [28, 29], suggested that fluorescence-related artifacts could be the cause of these apparent enhancements, as no substrate or product diffusion enhancement was observed in NMR diffusion measurements. Other studies that do not utilize FCS have also reported mixed results. Multiple studies have shown that enzymes attached to nanoparticles' surfaces can drive the motion of those particles. An enhanced diffusion coefficient for enzyme-powered particles on the nanometer and micrometer lengthscales was reported using particle tracking [2, 30, 31], and DLS [32], two techniques which are not affected by fluorescence artifacts. On the other hand, Chen [33], used an electrokinetic feedback trap to infer particle motions. Statistics would be much poorer than in DLS, but the technique is sensitive. No enhancement was seen in alkaline phosphatase, while a 20% enhancement was seen in parallel FCS measurements.

In this project, we are making alkaline phosphatase functionalized 200 nm in diameter spherical particles to study their enzyme activity and measure, using DDM and DLS, their diffusion coefficient. Without utilizing FCS artifacts and providing evidence that enzyme kinetics itself is actually happening, we will report whether the alkaline phosphatase functionalized particles are undergoing enhanced diffusion or not. We expect that particles in the nanoscale will be more affected by Brownian fluctuations than particles in the microscale, and therefore, this enhanced motion should appear as an enhanced diffusion coefficient. As the particles get smaller, we expect their diffusion to be more enhanced. However, the relation between particle size and diffusion enhancement is as yet unclear, in particular, because we do not know if the enzyme coverage is uniform and similar for particles of all sizes. Also, the enzyme activity as a function of those particles' size is still unknown.

Chapter 2

Colloidal Diffusion

Colloidal diffusion, the Brownian motion of particles in a colloidal system, can be measured using various techniques. These techniques include dynamic light scattering (DLS) [11], dynamic diffusion microscopy (DDM) [4], fluorescence correlation spectroscopy (FCS) [34], pulsed-gradient nuclear magnetic resonance (PG-NMR) [35], and fluorescence recovery after photobleaching (FRAP) [36]. In this work, we used the DDM and DLS techniques.

2.1 Diffusion and Size Measurements by DLS

We measured the diffusion coefficients for the size range of (1μm - 60nm) in diameter of spherical polystyrene particles purchased from Millipore Sigma dispersed in water using the Malvern Zetasizer Nano-ZS ZEN3600, which uses a red laser (λ =632.8nm) with a θ =175° angle of detection.

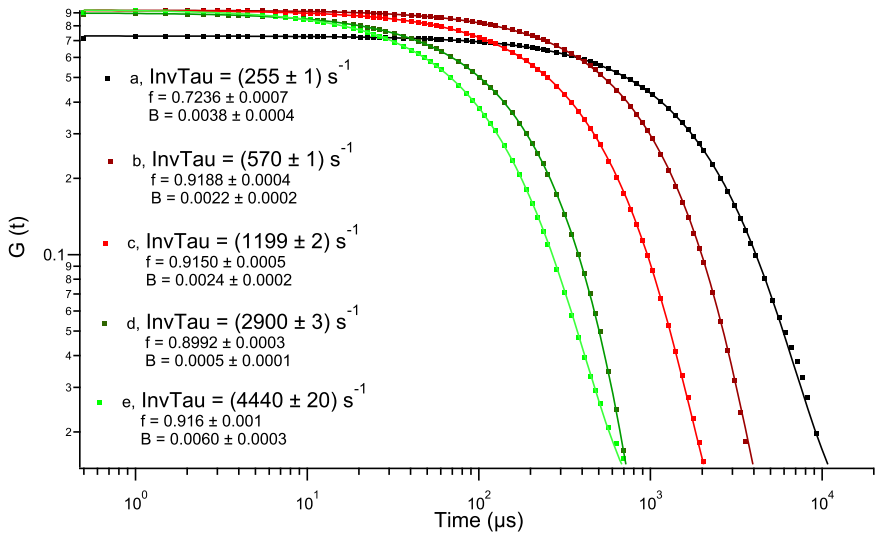

Figure 2.1: The auto-correlation of the scattered intensity of polystyrene spherical particles with a diameter of (a) 1μm, (b) 540nm, (c) 250nm, (d) 100nm and (c) 60nm dispersed in water at room temperature 24° C fitted to the mono-exponential equation 1.2, where $InvTau = Dq^2$.

In Figure 2.1, The auto-correlation function is curve-fitted to Equation 1.2. From the fit, we can use the diffusion coefficient with Stokes-Einstein Equation 1.1 to obtain the hydrodynamic diameter for nanoparticles in the size of $d > \lambda/10$. Otherwise, the scattered light will carry the same energy as the incident light (elastic scattering) and is no longer angle-dependent. This size threshold $d > \lambda/10$ is due to how electromagnetic waves (e.g., light) interact with a particle[37, 38]. The scattering vector q, was calculated using equation 1.3 and has a value $q = 2.64 \times 10^7$ m^{-1}. The diffusion coefficient D, and the hydrodynamic diameter d, using the Stokes-Einstein equation 1.1, are shown in Table 2.1.

Sample	Stated Diameter (nm)	Solid wt%	$InvTau$ (s^{-1})	D (m^2/s) $\times 10^{-15}$	d (nm)
a	1000	0.01%	255 ± 1	376 ± 2	1270 ± 10
b	540	0.01%	570 ± 1	819 ± 2	555 ± 7
c	250	0.01%	1199 ± 2	1720 ± 4	259 ± 2
d	100	0.1%	2900 ± 3	4050 ± 4	109 ± 3
e	60	0.125%	4440 ± 20	6370 ± 30	68 ± 1

Table 2.1: Diffusion and size results of polystyrene particles dispersed in water at room temperature 24° using DLS.

Commercial instruments such as the Malvern Zetasizer Nano-ZS ZEN3600 (the one used in this work) use the DLS technique together with built-in software to report nanoparticle size in an easy and quick way directly. However, we chose to extract the auto-correlation function, $G(t)$, and obtain the hydrodynamic diameter by directing fitting, i.e., in a comparable way to the differential dynamic microscopy (DDM) technique.

2.2 Diffusion and Size Measurements by DDM

In parallel with DLS measurements, in order to validate our DDM setup, we carried out a series of DDM measurements on the same polystyrene particles dispersed in water for the same size range (1 micron - 60 nm). All DDM experiments were done by capturing 10000 frames with a resolution of 256x256 pixel or (128x128 pixel for the 60nm particles) using the high speed camera pco.edge 4.2 LT equipped with a scientific CMOS sensor (up to 325 frames per second at 256x256 pixel, and 325 frames per second at 128x128 pixel) at room temperature (24° C), then calculating the images difference signal $S(\Delta t)$ in Fourier space for each time delay Δt using existing python code [5] written in a new python 3 implementation [39]. In Figure 2.2, the right image shows the intensity difference in real space between two frames, the left and the middle images, separated by a short time delay $\Delta t = 30.8$ ms.

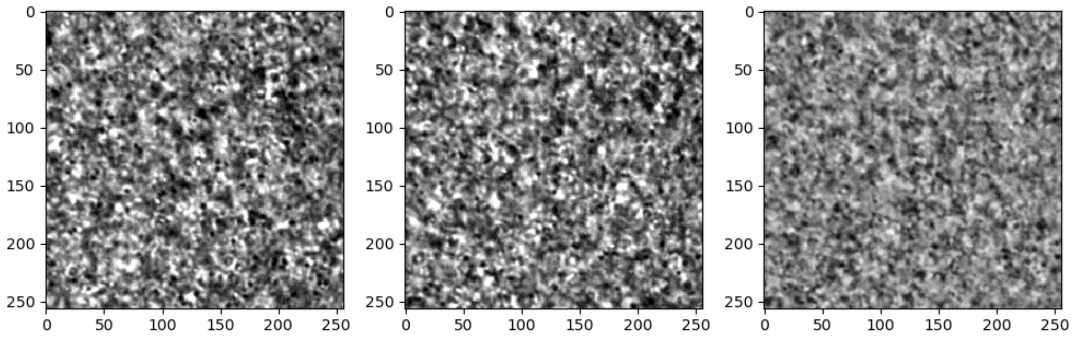

Figure 2.2: Image difference with a resolution of 256x256 pixel (162.5 nm/pixel) for 540nm diameter polystyrene particles dispersed in water captured by white-light microscopy using a 40x (NA = 1.00) oil-immersion objective. The left and middle images are two frames separated by 30.8 ms. The right image shows the intensity difference between those frames.

In Figure 2.3, the power spectra $|F_S(q;\Delta t)|^2$ are plotted as a function of time for a range of q values for the particle sizes 2.3a $d = 1\mu$m, 2.3b $d = 540$ nm, 2.3c $d = 250$ nm, 2.3d $d = 100$ nm, and 2.3e, 2.3f both are $d = 60$ nm. The black data corresponds to the smallest value of q, and the blue, red, and yellow data correspond to progressively larger values of q. As the value of q increases, the characteristic time of the power spectra decreases. This indicates that the samples are undergoing Brownian motion. in order to obtain the relation between q and the characteristic time $\tau(q)$, according to relation 1.7, the power spectra for the particles with a range of diameters varying from 1 μm to 250 nm were fitted to the mono-exponential function,

$$|F_S(q;\Delta t)|^2 = b(1 - a\exp(-\Delta t/\tau)). \tag{2.1}$$

The characteristic time $\tau(q)$, using the mono-exponential fit, for the particle diameters varying from 1 μm to 250 nm is attained. The inverse time τ^{-1} is plotted in Figure 2.4 as a function of q^2 for different particle sizes. It is clear that the dependency is fitted well by a linear relation between τ^{-1} and q^2 over a significant range of q^2 as shown in figures 2.4a, 2.4b and 2.4c representing τ^{-1} against q^2 for particle diameters $d = 1\mu$m, $d = 540$ nm and $d = 250$ nm. For the smaller sizes (100 nm and 60 nm), the mono-exponential fit gave inconsistent results (slower than expected), more likely due to colloidal aggregation and camera speed limitation. By fitting the power spectra versus time using a bi-exponential function we had two diffusion modes (a slow one for the aggregations and a fast one for the single particles). See figures 2.4d and 2.4e. The function utilized,

$$|F_S(q;\Delta t)|^2 = b[1 - a(pe^{-\Delta t/\tau_1} + (1-p)e^{-\Delta t/\tau_2})], \tag{2.2}$$

yielded a reasonable fit, and both the resulting times appeared to be associated with diffusive modes (i.e. $1/\tau$ vs q^2 was linear over a significant q range).

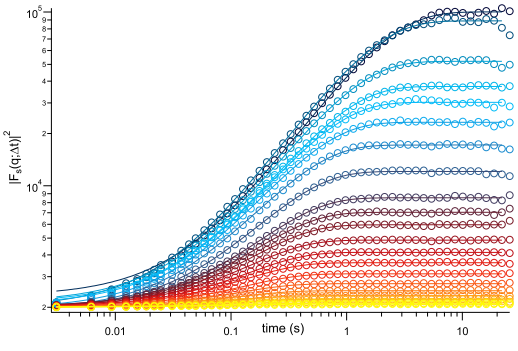

(a) Stated particle diameter $d = 1\mu$m

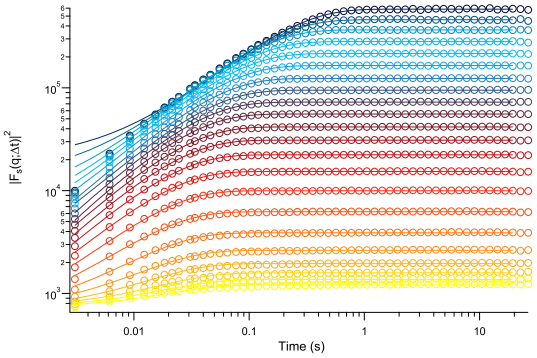

(b) Stated $d = 540$ nm

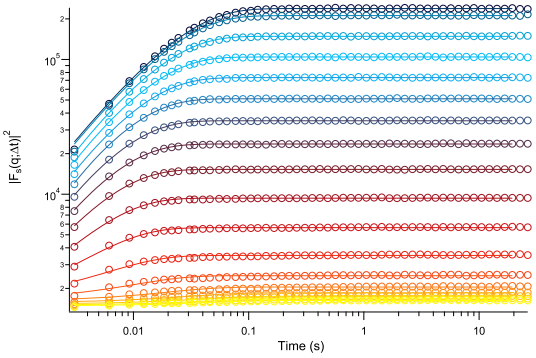

(c) Stated $d = 250$ nm

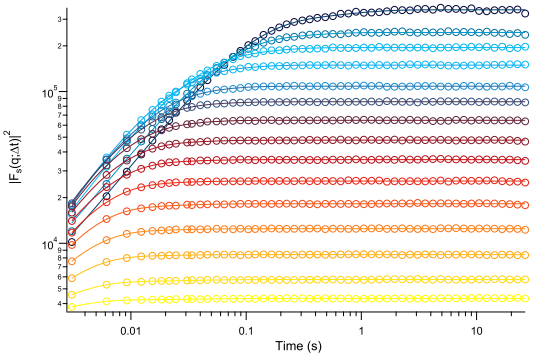

(d) Stated $d = 100$ nm

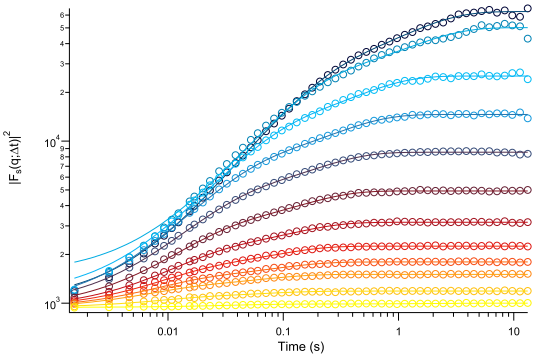

(e) Stated $d = 60$ nm, left side

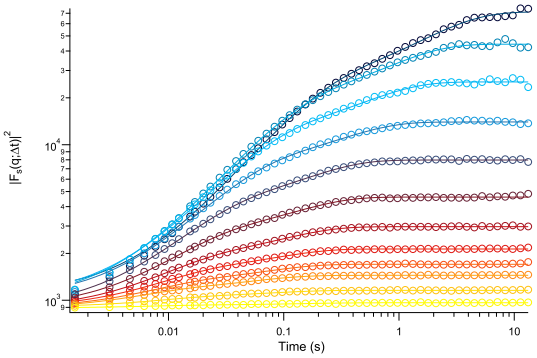

(f) Stated $d = 60$ nm, right side

Figure 2.3: Power spectra $|F_S(q;\Delta t)|^2$ versus time for polystyrene particles dispersed in water at room temperature 24° C. The colours contrast from blue to red to yellow, representing different q values from smaller to higher.

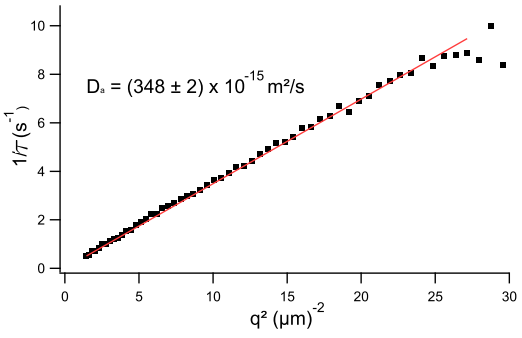

(a) Stated particle diameter $d = 1\mu$m

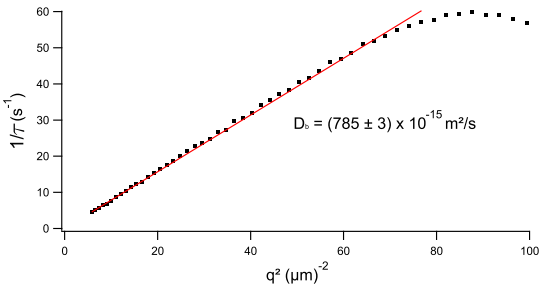

(b) Stated $d = 540$ nm

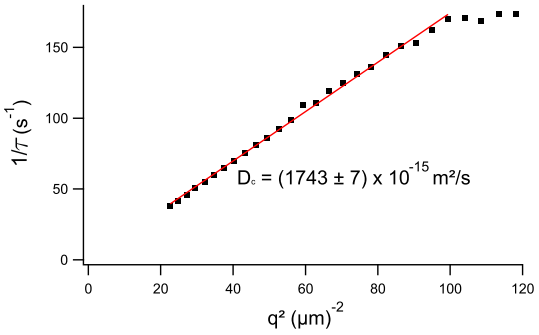

(c) Stated $d = 250$ nm

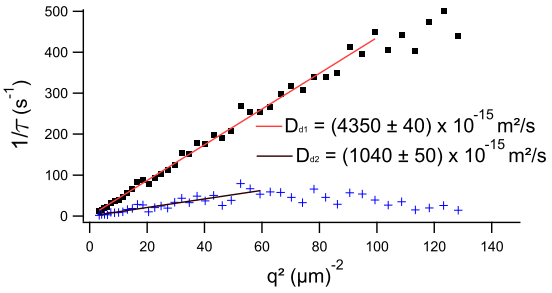

(d) Stated $d = 100$ nm

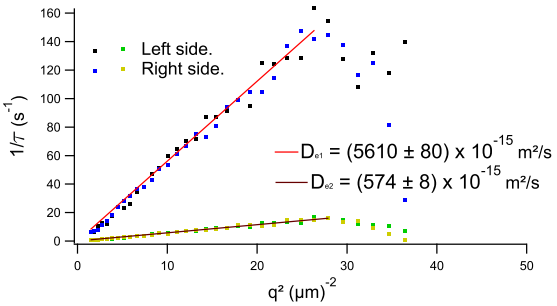

(e) Stated $d = 60$ nm

Figure 2.4: $1/\tau(q)$ vs q^2 yields diffusion coefficients (in units of 10^{-15}m^2/s). In addition to the primary size, there is a second diffusion mode of larger particles for (d) and (e).

The sequence of images for the particles of (1 μm - 100) diameter was captured at 256x256 pixel resolution with an acquisition speed of 325 frames per second (FPS). As the smaller 60 nm particles diffuse faster, they require a higher frame rate. We managed to double the frame rate to 650 FPS by lowering the resolution to 128x128 pixel. In order to compensate for the poorer statistics, we analyzed a wide 128x256 pixel sequence as two 128x128 pixel sequences separately. The figures 2.3e and 2.3f, show the power spectra of the wide image split into two images (left side and right side), where Figure 2.4e, shows the average diffusion coefficients of the two sides.

Using the Stokes-Einstein relation (equation 1.1), the calculated particles' hydrodynamic diameter are shown in the following table:

1	2	3	4	5	6	7	8
Sample	Stated Diameter (nm)	d_{DLS}(nm)	Solid wt%	D (m^2/s) $\times 10^{-15}$	d(nm)	D_2 (m^2/s) $\times 10^{-15}$	d_2 (nm)
a	1000	1270 ± 10	0.1%	348 ± 2	1265 ± 10	-	-
b	540	555 ± 7	0.5%	785 ± 3	556 ± 6	-	-
c	250	259 ± 2	1%	1743 ± 7	259 ± 3	-	-
d	100	109 ± 3	2.5%	4350 ± 40	104 ± 2	1040 ± 50	440 ± 20
e	60	68 ± 1	2.5%	5610 ± 80	75 ± 2	574 ± 8	730 ± 10

Table 2.2: Diffusion and size results of polystyrene particles dispersed in water at room temperature 24° C using DDM.

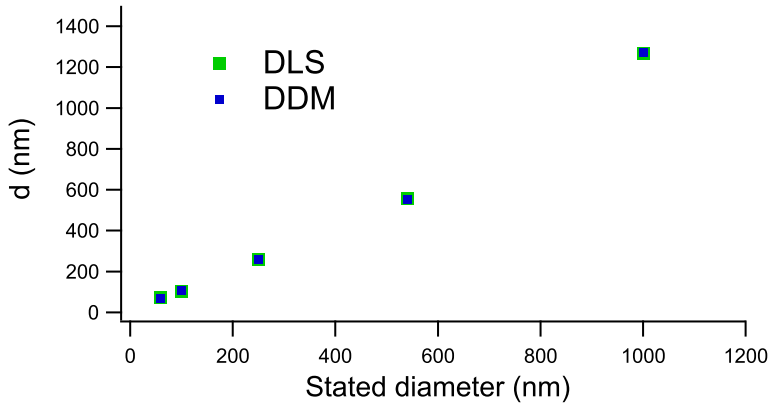

Figure 2.5: The measured hydrodynamic diameter, using DLS and DDM, against the stated diameter. Errors are smaller than the symbol size.

2.3 Conclusion

Differential dynamic microscopy (DDM) was found to be a robust and valid technique to study the dynamical behaviour of a colloidal dispersion for the size range of (1 μm - 100 nm) that provides reasonably good statistics provided that we are recording a large enough field of the sample (see figure 2.2). For the smaller size particles (60 nm in diameter), it was challenging to achieve precise measurements due to the faster diffusion of the particles. In this case, we had to pick a smaller field of the sample in order to increase the camera frame rate. Also, the polydispersity for the small sizes (100 nm and 60 nm) led to a slight disagreement with the DLS results. But overall, the DDM shows strong agreement with the DLS results as columns 3 and 6 show in Table 2.2. Moreover, this technique is compatible with microfluidic geometries, which are of interest in future experiments.

Chapter 3

Alkaline Phosphatase Kinetics

3.1 Michaelis-Menten Constants for Alkaline Phosphatase

The goal of measuring the alkaline phosphatase kinetics constants is to understand the bare alkaline phosphatase kinetics and build the groundwork for comparison with the kinetics discussed in the next chapter for alkaline-phosphatase-functionalized nanoparticles. These functionalized nanoparticles are basically spherical polystyrene nanoparticles coated (by attaching to a linker molecule) with alkaline phosphatase. One potential challenge with using enzymes attached to nanoparticles is that the enzyme concentration may be low, due to small enzyme coverage on the surface of the particles, which increases their activity time scale. Therefore, it is convenient to find a medium in which the enzyme activity is faster.

Enzyme activity depends sensitively on the environment of the reaction medium. This environment includes the temperature, the pH value, and the concentrations of certain salts that work as co-factors for that enzyme. The enzyme alkaline phosphatase has a maximum activity at an optimum pH value that ranges from 7.5 pH to 9.5 pH [40]. We studied the alkaline phosphatase in two different buffers: 0.2 M phosphate buffer at 7.0 pH, and 1 M tris-HCl buffer at 7.5 pH. All measurements were done at 25 °C using the SYNERGY Mx multi-plate reader, which offers the opportunity to use smaller volumes of samples as well as to run multiple measurements simultaneously, by adding 100 μL of the alkaline phosphatase solution to 100 μL of its substrate (pNPP) solution for each different substrate concentration. The data interval for each absorbance against time point was 10 seconds (6 points per minute). When measuring enzyme kinetics, it is important to consider the time gap between mixing the sample and starting data acquisition. This time gap, also known as the "lag time," can affect the accuracy of the measurements. In general, the lag time should be kept as short as possible to ensure that the measurements are accurate. However, in some cases, it may be necessary to allow for a longer lag time to ensure that the reaction has progressed to a measurable level.

The alkaline phosphatase used in this work, purchased from Millipore Sigma, supplied as a solution in 40% glycerol containing 6 mM Tris, 6 mM $MgCl_2$ and 0.12 mM $ZnCl_2$, 7.6 pH was divided into multiple vials and stored at temperature 4°C. The substrate pNPP, purchased from Millipore Sigma in powder shape, was stored at temperature 4°C. Measurements were done on freshly prepared samples from pNPP powder and alkaline phosphatase solution as supplied.

3.1.1 Alkaline Phosphatase Kinetics in Phosphate Buffer

Referring to Figure 1.4, in Section 1.4.2, the product (pNP) absorbance peak was at $\lambda_{max} = 400$ nm. However, we found that at $\lambda = 400$ nm the absorbance peak of the product (pNP) interferes with the tail of the absorbance of the substrate (pNPP). This is seen clearly in Figure 3.1a. In order to make sure that this interference would not affect the results, we did multiple measurements at different wavelengths (400 nm, 425 nm, and 450 nm). In those measurements, the absorbance was plotted against time and found to be linear as shown in Figures 3.1a, 3.1b and 3.1c. If the reaction is proceeding at a constant rate, the plot will be linear, with a slope that represents the reaction rate. To obtain the reaction rate, the data were linearly fitted. Once the reaction rate has been determined, it can be plotted against the substrate concentration on a Michaelis-Menten graph to obtain the enzyme kinetics constant as shown in Figures 3.1d, 3.1e and 3.1f. By fitting the data to the Michaelis-Menten equation 1.23, it is possible to obtain the enzyme kinetics constant, K_m.

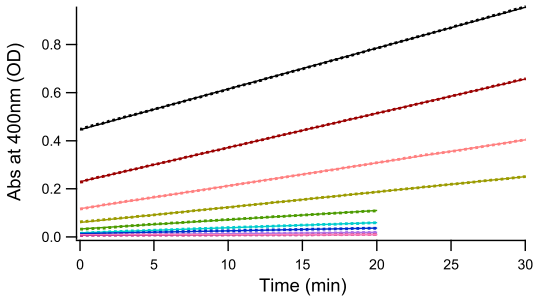

(a) Absorbance against time at $\lambda_{max} = 400$ nm.

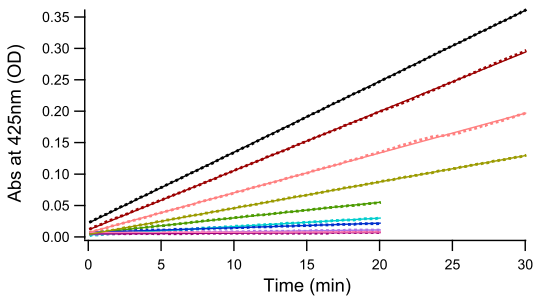

(b) Absorbance against time at $\lambda = 425$ nm.

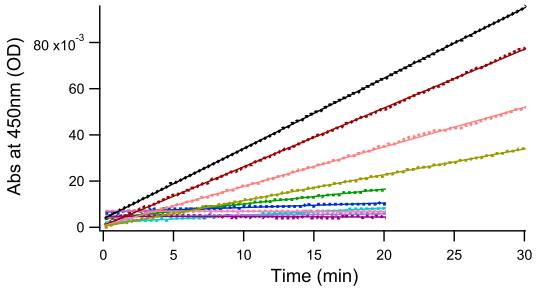

(c) Absorbance against time at $\lambda = 450$ nm.

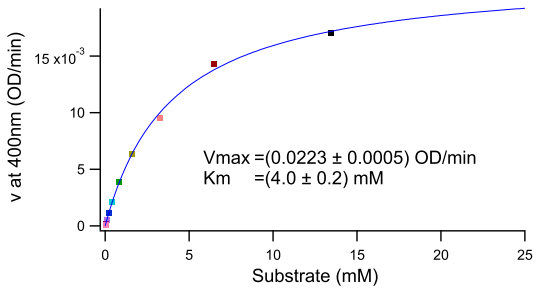

(d) Michaelis–Menten plot at $\lambda_{max} = 400$ nm.

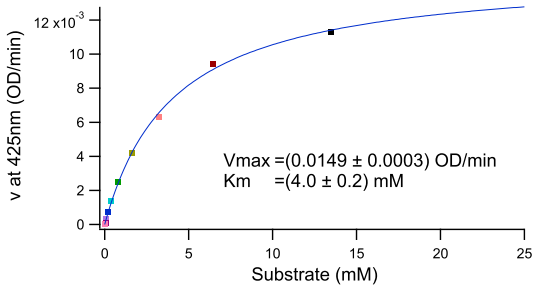

(e) Michaelis–Menten plot at $\lambda = 425$ nm.

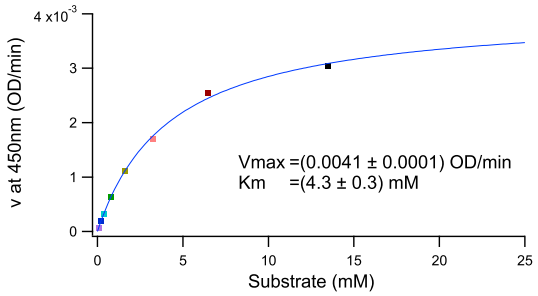

(f) Michaelis–Menten plot at $\lambda = 450$ nm.

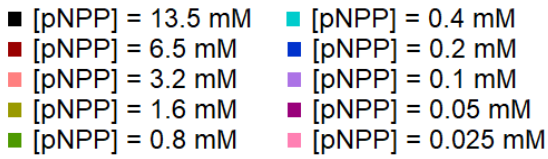

(g) Substrate concentration colours indicator.

Figure 3.1: Alkaline phosphatase kinetics in 0.2 M phosphate buffer at 7.0 pH and 25 °C, containing 2 nM of 6630 U/mg alkaline phosphatase and (0.025 mM, 0.05 mM, 0.1 mM, 0.2 mM, 0.4 mM, 0.8 mM, 1.6 mM, 3.2 mM, 6.5 mM, and 13.5 mM) of pNPP.

The Michaelis–Menten constant K_m ≈4.0 mM, was found to be consistent across the three different wavelengths, where the maximum reaction rate V_{max} decreased as we move away from the peak absorbance wavelength λ_{max}.

Figure 3.2 displays the absorbance spectra of the substrate pNPP at three known concentrations. The inset of the figure emphasizes the tail of the curves, revealing that a substantial contribution to the signal from the substrate is still present at 400 nm, yet diminishes significantly beyond 420 nm. While there is a slight increase in absorbance above 420nm, it is insignificant and could be attributed to background correction. This observation indicates that the signal at wavelengths above 420 nm is less likely to interfere with the substrate pNPP spectrum.

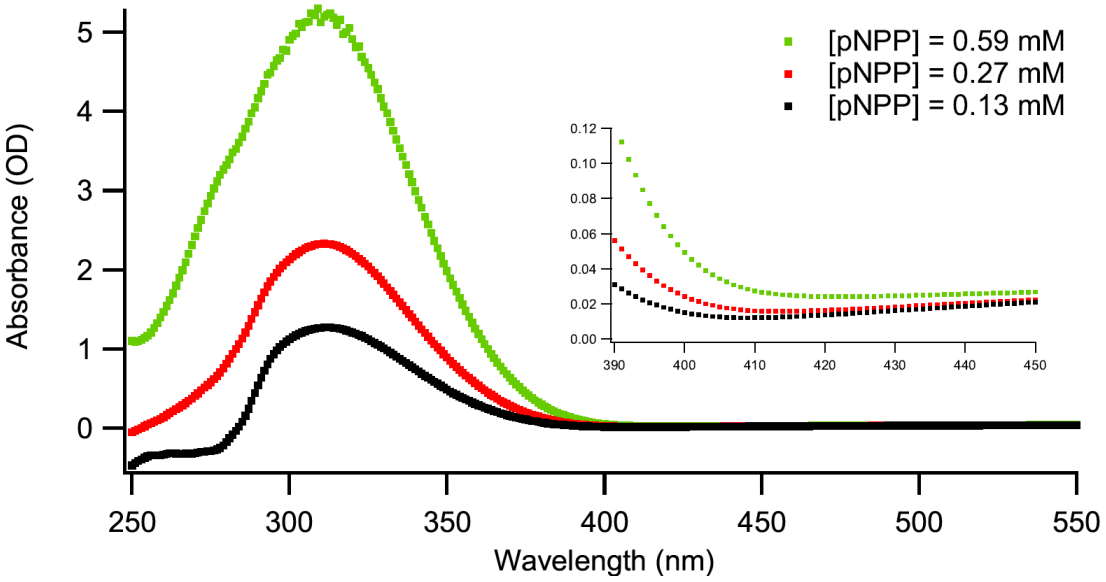

Figure 3.2: The substrate pNPP in tris-HCl buffer at 7.6 pH spectrum shows absorbance at $\lambda = 400$ nm that indicates the observed interference in Figure 3.1a.

3.1.2 Alkaline Phosphatase Kinetics in Tris-HCl Buffer

As mentioned earlier, alkaline phosphatase is an enzyme that functions optimally at a pH of 7.5 - 9.0, so it is expected to have higher activity in a tris-HCl buffer at a pH of 7.6 compared to a phosphate buffer at a pH of 7.0. However, it is also essential to consider other factors that may affect enzyme activity, such as the presence of inhibitors or activators and the ionic strength of the solution. These factors may also contribute to any differences in enzyme activity observed between the tris-HCl buffer and the phosphate buffer.

The enzyme alkaline phosphatase was studied in a tris-HCl buffer at pH 7.6 and 25°C. The kinetics of the enzyme were determined by measuring the absorbance at 400 nm over time. It was observed that the absorbance was linear at short times (< 4 min), but eventually saturated as seen in the green and blue curves in Figure 3.3a, which correspond to lower substrate concentration. The reaction rates were measured by linearly fitting the data at small time values and then plotting the reaction rate v (in the units of OD/min) against substrate concentration on a Michaelis-Menten plot as shown in Figure 3.3b. The data were fit to the Michaelis-Menten equation 1.23, allowing the determination of the kinetic constants that were found to be consistent with other published work [40].

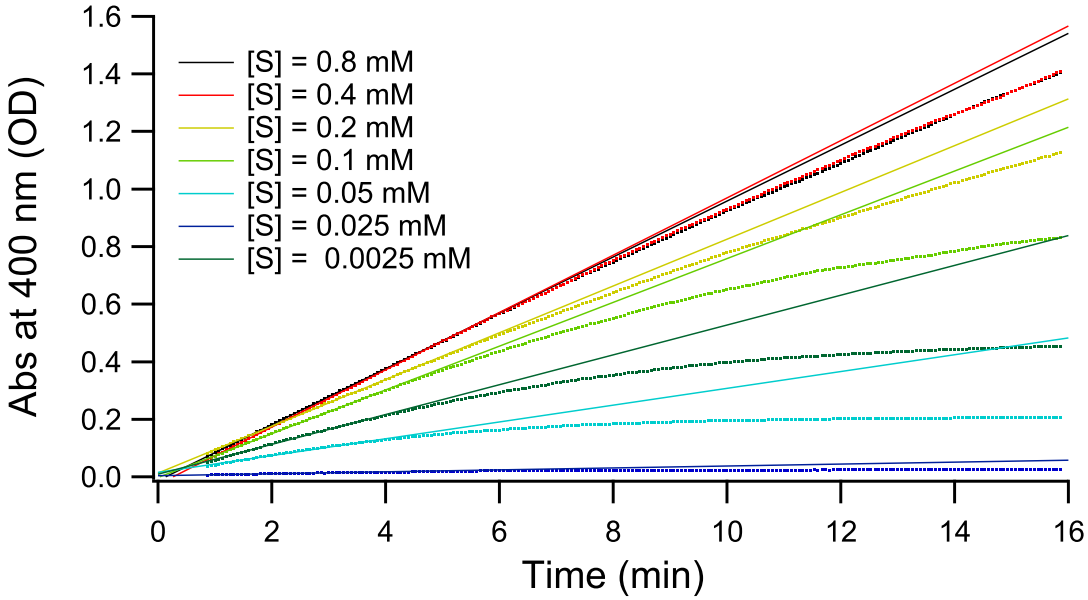

(a) Absorbance against time at $\lambda_{max} = 400$ nm.

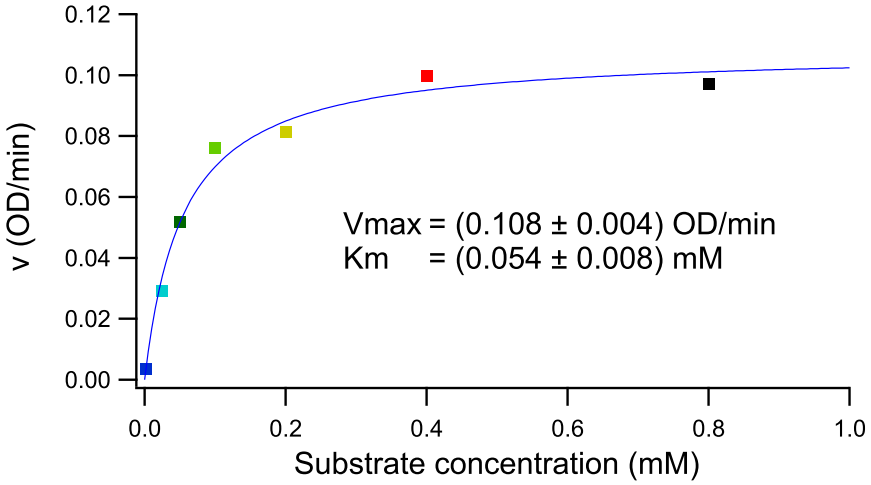

(b) Michaelis–Menten plot at $\lambda_{max} = 400$ nm. The colours in (b) are coordinated with these in (a).

Figure 3.3: Alkaline phosphatase kinetics in 1 M tris-HCl buffer at 7.6 pH and 25 °C, containing 0.2 nM of 6630 U/mg alkaline phosphatase and (0.0025 mM, 0.025 mM, 0.05 mM, 0.1 mM, 0.2 mM, 0.4 mM, 0.8 mM) of pNPP.

Alkaline phosphatase was found to be much more active in tris-HCl buffer at 7.6 pH and the same 25 °C temperature. The obtained Michaelis–Menten constant in tris-buffer K_m ≈0.05 mM (much lower than 5 mM in phosphate buffer), indicates that alkaline phosphatase has more affinity to its substrate in the tris-HCl buffer. The higher alkaline phosphatase activity requires a much smaller amount of its substrate (pNPP) to study its kinetics. Here, we used a range from 0.0025 mM to 0.8 mM. For such a small amount of pNPP, the interference issue at $\lambda_{max} = 400$ nm is negligible and did not appear in Figure 3.3a.

3.2 Conclusion

Measuring the increase of the yellow pNP product (i.e. the reaction rate v) by spectroscopy during the alkaline phosphatase catalyzed reaction at a fixed alkaline phosphatase concentration with different substrate (pNPP) concentrations yields a correlation between the substrate concentration and reaction rate v that follows the Michaelis–Menten relation. Michaelis–Menten constant (K_m) for alkaline phosphatase; the inverse measure of alkaline phosphatase affinity for its substrate pNPP obtained by fitting the reaction rate v against substrate concentration, found to be much lower in tris-HCl buffer at 7.5 pH than it was in phosphate buffer at 7.0 pH (0.05 mM $>$ 4 mM). Since alkaline phosphatase appears to be much more active in tris-HCl buffer, we were able to study its kinetics at low enzyme concentration (0.2 nM) compared to phosphate buffer (2 nM), which becomes handy when studying the enzyme activity of an alkaline phosphatase functionalized colloids in the next chapter. Shifting away from the absorbance peak λ_{max} of the product (pNP) in order to avoid the absorption interference of the substrate (pNPP) with the product (pNP) gave consistent results of the Michaelis–Menten constant (K_m= 4 mM) in phosphate buffer at the three absorbance wavelengths (400 nm, 425 nm, 450 nm) with the highest wavelength showing the least overlay with substrate absorbance. In tris-HCl buffer, the absorption interference between the substrate (pNPP) and the product (pNP) was negligible due to using a small amount of the substrate in the solution.

Chapter 4

Alkaline Phosphatase Functionalized nanoparticles

4.1 Alkaline Phosphatase Glutaraldehyde Coupling to Nanoparticles

The nanoparticles used in this study are 200 nm diameter spheres purchased from MilliporeSigma with amine group surface functionalization. The alkaline phosphatase molecules were attached to the nanoparticles' surface using glutaraldehyde coupling. The reaction of binding the alkaline phosphatase enzyme to a 200 nm diameter nanoparticle is shown in Figure 4.1. The glutaraldehyde attaches to an amine group on the surface of the nanoparticles in step A. The glutaraldehyde then binds to an amine group on the alkaline phosphatase enzyme in step B. Step C simply highlights that most amine groups on a nanoparticle's surface are enzyme functionalized, as in step B. Polysciences Inc [8], used to sell a glutaraldehyde coupling kit with a hollow fibre filtering system that is suitable for attaching proteins to nanoparticles. Unfortunately, this product is discontinued and not available anymore. However, we followed their protocol in order to attach the alkaline phosphatase molecules to the particles.

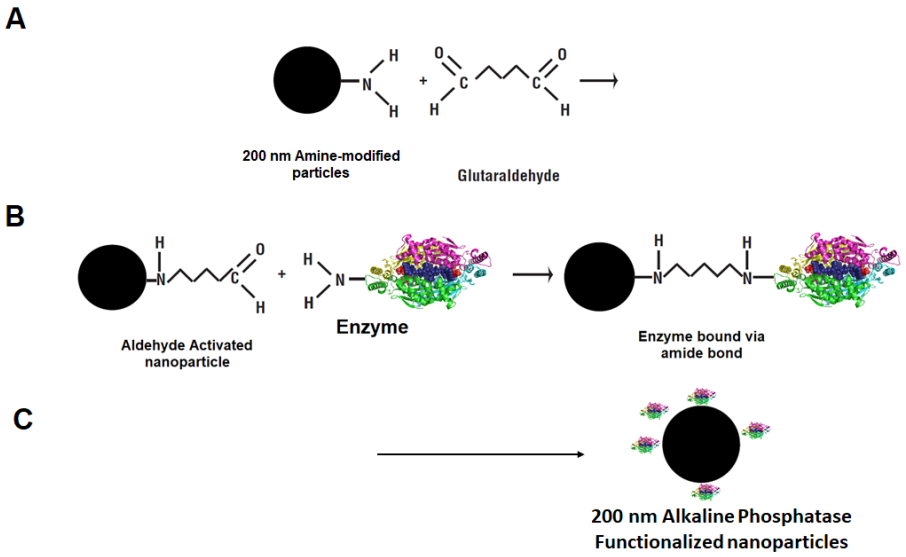

Figure 4.1: Attachment of the enzyme alkaline phosphatase on 200 nm particles. A) Glutaraldehyde binds to the amine group on the surface of the particles, B) Glutaraldehyde binds to the amine group on the enzyme, C) The reactions in (A) and (B) occur many times, in parallel, to coat the particles with enzymes giving a 200 nm alkaline phosphatase functionalized nanoparticles. The Enzyme structure in the graph was extracted from the PDB file [7], and the chemical structures are adopted from the technical data sheet [8].

4.1.1 Synthesis of Alkaline Phosphatase Functionalized nanoparticles

This section presents a comprehensive guide to the synthesis of AP-functionalized nanoparticles, which is elaborated in detail in the Appendix 5.1.

The protocol involves the use of six solutions, referred to as vial A, vial B, vial C, vial D, vial E, and vial F. Vial A is a solution of 16.6 mg/ml of 200 nm amine-functionalized polystyrene nanoparticles in Dulbecco's phosphate-buffered saline (DPBS). Vial B is a solution of 18% glutaraldehyde in DPBS. Vial C is an alkaline phosphatase solution at a concentration of 1.84 mg/ml or 13.14 mM (12.5 kU/ml) in DPBS. Vial D is a solution of 0.2 M ethanolamine in DPBS. Vial E is a solution of 1 mg/ml of Bovine Serum Albumin (BSA) in DPBS. Vial F is a solution of Tris-HCl buffer at pH 7.6.

A series of chemical and physical steps were used to synthesize alkaline phosphatase functionalized nanoparticles. Vial A, containing 16.6 mg/ml of 200 nm amine-functionalized polystyrene nanoparticles in DPBS, was mixed with vial B, containing 18% glutaraldehyde in DPBS. The solution was rotated at room temperature for 6 hours, allowing the glutaraldehyde molecules to react with the amino groups on the nanoparticles' surface. The solution was then centrifuged and redispersed in DPBS several times, followed by treatment with ultrasound waves using

an ultrasonic bath for 3 minutes. Vial C, containing 0.43 ml of alkaline phosphatase at a concentration of 1.84 mg/ml or 13.14 mM (12.5 kU/ml) in DPBS, was then added to the solution and rotated at room temperature for 18 hours, allowing the enzyme molecules to react with the glutaraldehyde molecules on the nanoparticles' surface. The solution was mixed with vial D, containing 0.2 M ethanolamine in DPBS for 30 minutes, to block unreacted sites on the nanoparticles' surface. The solution was washed several times with vial E, containing 1 mg/ml of BSA in DPBS, BSA blocks any remaining polymer particle surfaces and minimizes nonspecific protein binding in downstream assays. Finally, the solution was washed with vial F, containing 0.1 M Tris-HCl buffer at pH 7.6, to remove excess reagents or contaminants. The final sample was alkaline phosphatase functionalized nanoparticles in Tris-HCl buffer, with a concentration of 7.14 mg/ml and a particle size of 200 nm.

4.2 (Alkaline Phosphatase)-nano Particles Enzyme Activity and Diffusivity

At this point, we can not be sure whether we successfully functionalized our particles with enzymes or not. However, if the particles show enzymatic activity, that will be a robust clue that indicates the success of our protocol.

4.2.1 Enzyme Activity

Before testing the enzymatic activity of our alkaline phosphatase functionalized particles, it is necessary to exclude any other enzymatic activities associated with the free enzymes if they exist in the sample or with the nanoparticles if they catalyze the reaction. We tested the enzymatic activity of the supernatant after washing the particles multiple times in tris-HCl buffer 1 M, pH 7.6 at room temperature by mixing it with the substrate p-nitrophenylphosphate (pNPP) where the final substrate concentration is 7.07 mM. Also, an enzyme activity test was done on the bare amine-modified 200 nm nanoparticles in tris-HCl buffer 1 M, pH 7.6 at room temperature by mixing them with 7.07 mM of the substrate. Figure 4.2a shows the results of measuring the absorbance of the supernatant with the substrate pNPP at 400 nm wavelength over time, using a Cary 6000i UV-Vis Spectrometer. The graph indicates that there is a minimal decrease in absorbance after 0.5 minutes, likely due to background correction, but no increase in absorbance is observed. Similarly, Figure 4.2b presents the absorbance of bare 200 nm nanoparticles with the presence of the substrate pNPP at 400 nm wavelength against time, measured using the same Cary 6000i UV-Vis Spectrometer. This graph also shows no increase in absorbance over time. It is important to note that figures 4.2a and 4.2b have a vertical absorbance scale of 40×10^{-3}. Therefore, any slight variations observed in these figures will be lost in the noise of subsequent figures. Both supernatant and bare particles show no enzymatic activities as shown in Figure 4.2, which means any other enzymatic activity may show up when testing the functionalized particles is

exclusive for the attached alkaline phosphatase on the particles.

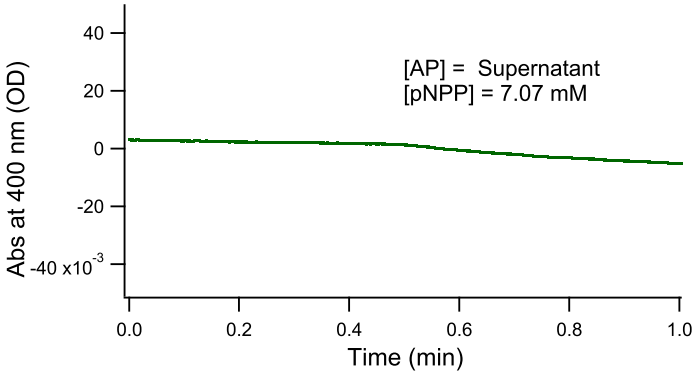

(a) The fourth supernatant and 7.07 mM of pNPP in tris-HCl buffer 1 M, pH 7.6.

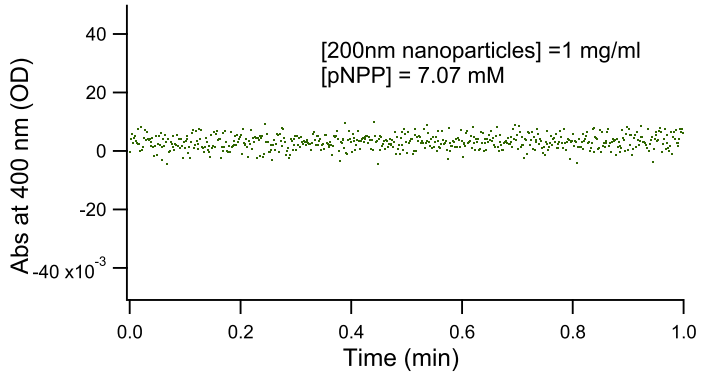

(b) 1 mg/ml of bare amine modified 200 nm nanoparticles and 7.07 mM of pNPP in tris-HCl buffer 1 M, pH 7.6.

Figure 4.2: The absorbance at 400 nm over time for the solutions (a) and (b), indicates the absence of enzymatic activity at temperature 24° C.

A test of enzymatic activity on the alkaline phosphatase functionalized particles was carried out by dispersing the functionalized particles in tris-HCl 1 M, pH 7.6, at 25°, then adding different amounts of the substrate pNPP while keeping the functionalized particles concentration fixed at 0.1 mg/ml. In Figure 4.3a, the absorbance at 400 nm wavelength over time is plotted for multiple samples with varying substrate concentrations and a fixed concentration of functionalized particles. The graph demonstrates that as time progresses, the absorbance of the samples increases linearly. In contrast with bare alkaline phosphatase kinetics shown in Figure 3.3a where the linear region extends to about 4 minutes, here it seems to extend to at least 15 minutes. Figure 4.3b shows the reaction rate calculated using the slopes from Figure 4.3a, plotted against the substrate concentration. A significant increase of the absorbance at $\lambda = 400$ nm was observed, and hence there is an enzymatic activity associated with the functionalized particles. By fitting the reaction rates against substrate concentration, the Michaelis–Menten constant $K_m = (0.065 \pm 0.004)$ mM, was found to be consistent with bare alkaline phosphatase, $K_m = (0.054 \pm 0.008)$ mM. However, the maximum reaction rate V_{max} is about a factor of 10, smaller than

for bare alkaline phosphatase.

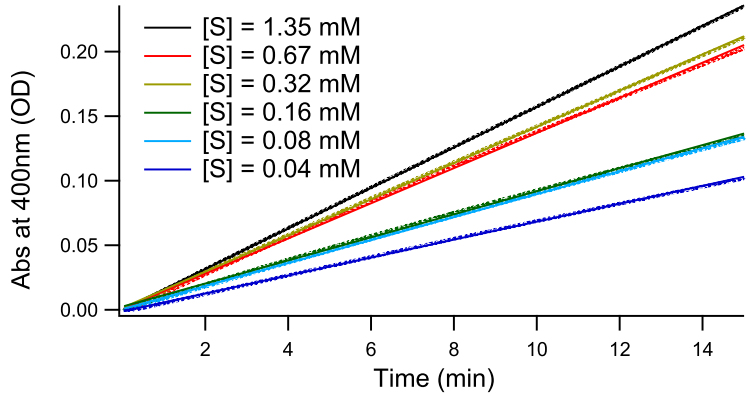

(a) Absorbance against time.

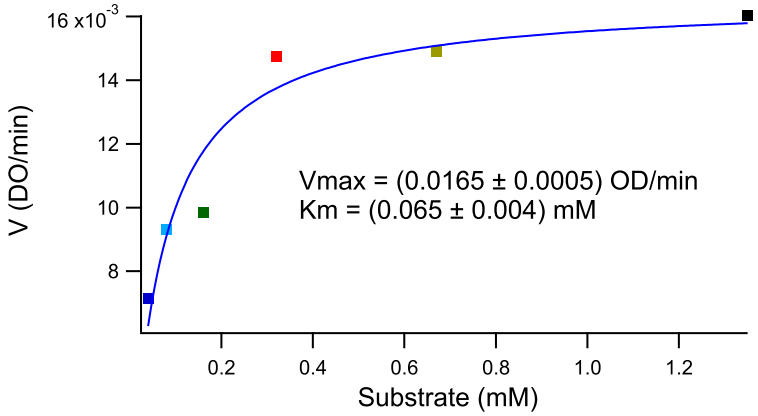

(b) Michaelis–Menten plot. The colours in (b) are coordinated with these in (a).

Figure 4.3: Alkaline phosphatase functionalized particles kinetics in 1 M of tris-HCl buffer, pH 7.6 at 25°, at functionalized particles concentration 0.1 mg/ml with substrate concentrations 0.04 mM, 0.08 mM, 0.16mM, 0.32 mM, 0.67 mM and 1.35 mM.

Since enzymes are attached to 200 nm size particles, it is fairly easy to collect those enzyme functionalized particles by centrifuging them after they catalyze the reaction, while collecting tiny bare alkaline phosphatase (≈140 kDa) is a much more complicated process. Since enzymes are not used up by the reaction and can be re-used again, we expect the enzyme functionalized particles to be recoverable. In other words, these particles are capable of catalyzing the reaction over and over. The alkaline phosphatase functionalized particles were collected after catalysis during the enzyme kinetics measurement, shown in Figure 4.3, by centrifuging the solutions for 15 minutes at 10°C and then re-dispersing them in 1 M of tris-HCl buffer at 7.6 pH. By measuring the recovered enzyme functionalized particles' kinetics, the kinetics constant, $K_m = (0.063 \pm 0.005)$ mM, was found to be the same as the first use constant. By recovering the enzyme functionalized particles multiple times and measuring their kinetics, the constant K_m was the same as shown in Figure4.4 which shows the Michaelis-Menten plots for the recovered, once and four times, alkaline

phosphatase functionalized particles compared to the Michaelis-Menten plot of the original alkaline phosphatase functionalized particles carried out from Figure 4.3b. However, the constant V_{max} is getting smaller each recovery, most likely due to losing some enzyme functionalized particles during the recovery process. With that being said, our alkaline phosphatase functionalized particles are easily recoverable and can be reused.

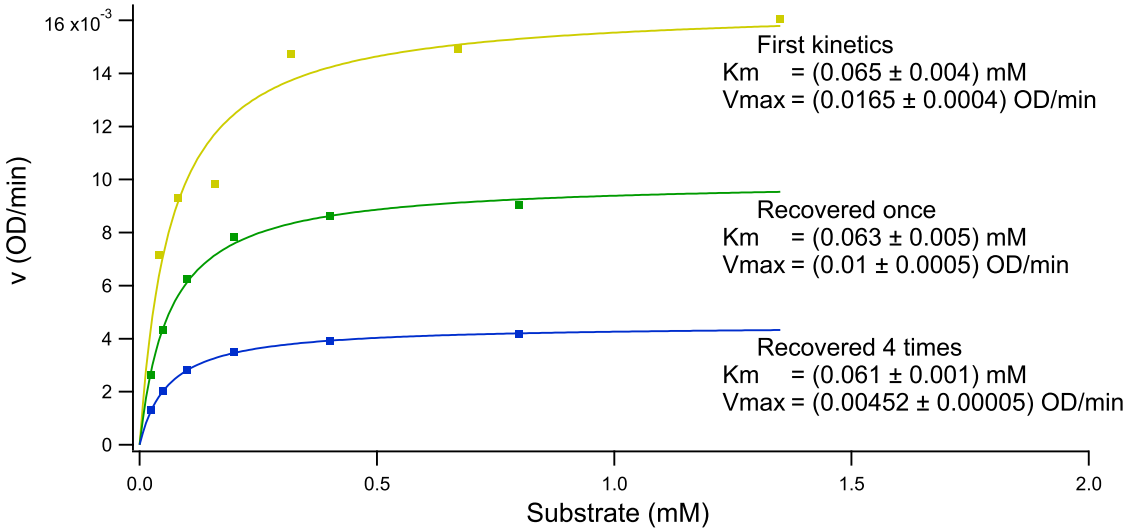

Figure 4.4: Michaelis–Menten plot for first used, recovered once and recovered four times alkaline phosphatase functionalized particles.

4.2.2 Diffusivity

After successfully attaching alkaline phosphatase to spherical 200 nm particles, the main question is whether DDM and DLS can observe enhanced diffusion. In order to build a ground for comparison, the diffusion coefficients were measured for the bare 200 nm particles, and the alkaline phosphatase functionalized particles dispersed in tris-HCl buffer at 7.6 pH. Then, by mixing the alkaline-phosphatase-functionalized particles with the substrate pNPP in tris-HCl buffer at 7.6 pH with final concentrations of 1 mg/ml and 1.35 mM of the functionalized particles and the substrate pNPP, the diffusion coefficient during catalysis was measured using DDM. The solution after the experiment was yellow, which means the functionalized particles were catalyzing the reaction. However, the diffusion coefficient results in Figure 4.5 which shows the diffusion coefficient of the bare nanoparticles, alkaline phosphatase functionalized nanoparticles without the substrate pNPP, and alkaline phosphatase functionalized particles over time during catalysis show no enhancement in the diffusion during catalysis. By repeating the measurements using DLS at concentrations 0.15 mg/ml and 0.62 mM for the functionalized particles and the substrate pNPP, no enhanced diffusion was observed as shown in Figure 4.6.

Notably, there is a small decrease in the diffusion coefficient from colloid to alkaline phosphatase functionalized colloid. This decrease is about 5% and could arise from a small increase in the hydrodynamic radius due to enzyme functionalization.

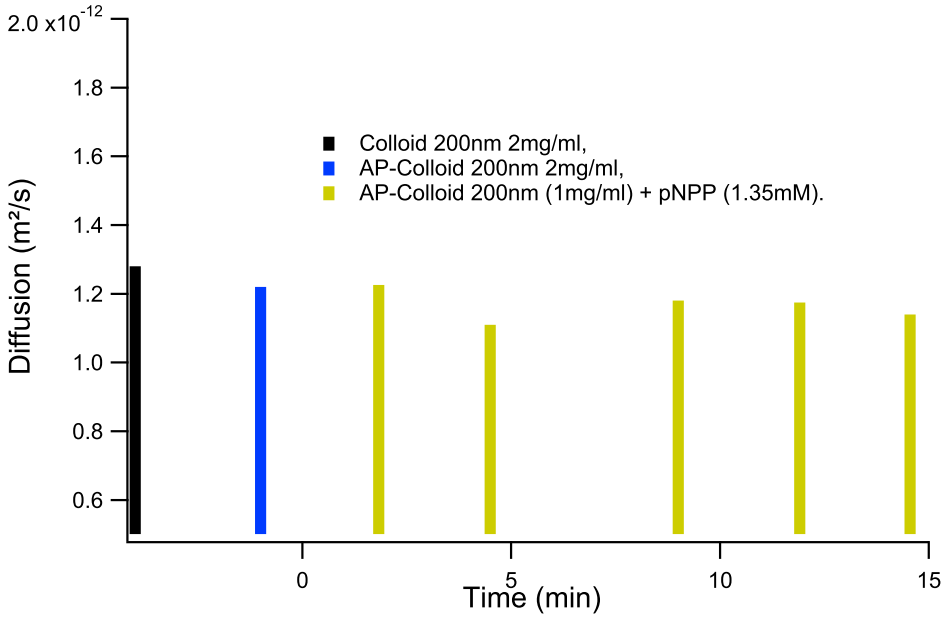

Figure 4.5: Diffusion coefficient by DDM for 200 nm bare particles (black), 200 nm alkaline phosphatase functionalized particles (blue) and 200 nm alkaline phosphatase functionalized particles during catalysis (yellow).

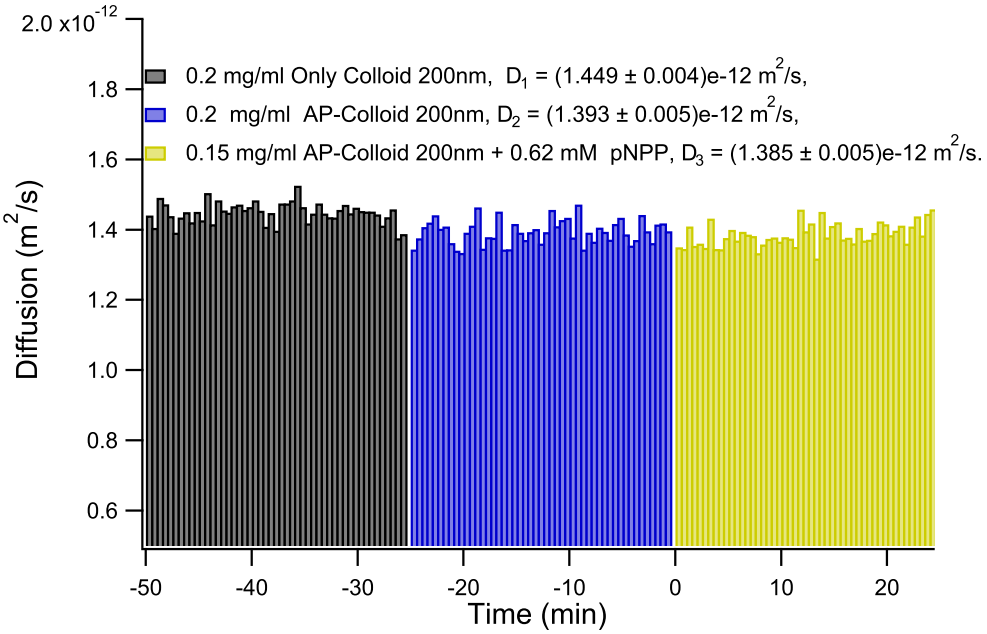

Figure 4.6: Diffusion coefficient by DLS for 200 nm bare particles (black), 200 nm alkaline phosphatase functionalized particles (blue) and 200 nm alkaline phosphatase functionalized particles during catalysis (yellow).

The absence of enhancement in the diffusion coefficient shown in Figures 4.5 and 4.6 could be due to a combination of uniformly distributed enzymes on the particles and small enzyme coverage on the particles. However, one of those possibilities can be excluded, as we will discuss in the future work Section 4.4. Moreover, perhaps

the energy arising from the enzyme-complex coming apart is not enough to push the particles, where the observed enhancements in the diffusion using FCS mentioned in Section 1.5 maybe come from the artifacts of dissociation and surface binding, as was suggested by Gunther et al [28, 29].

4.3 Conclusion

Amine-modified polystyrene spherical particles with 200 nm diameter, were successfully functionalized with alkaline phosphatase using glutaraldehyde coupling. It was fascinating to see the enzymatic activity of the functionalized particles with kinetics constant, $K_m = (0.065 \pm 0.004)$ mM, roughly the same as the bare alkaline phosphatase, $K_m = (0.054 \pm 0.008)$ mM. Even after recovering and washing the particles multiple times, their enzymatic activity was the same as the fresh functionalized particles. After confirming at the same time that the enzymes were catalyzing substrate effectively under nearly identical conditions and samples as the diffusion measurements, no enhancement in the diffusion coefficient of 200 nm alkaline phosphatase functionalized particles was observed during catalysis using DLS and DDM.

4.4 Future Work

As a next step in our research, we plan to explore the functionalization of particles with enzymes other than alkaline phosphatase. We will specifically look into the enzyme urease, which was used in the initial few studies that claimed an enhanced enzyme diffusion during catalysis. We will use a combination of different methods, including the FCS method and non-FCS methods such as dynamic light scattering (DLS) and dynamic diffusion microscopy (DDM), to assess the validity of this effect. We can better understand the diffusion behaviour of the enzyme during catalysis and establish whether any reported improvements are caused by real effects or fluorescence-related errors by comparing the data from these various techniques.

In addition to studying the functionalization of particles with various enzymes, we also intend to look at the impact of particle size on any enhancements in diffusion that may occur during catalysis. We want to explore the enhanced diffusion of various-sized functionalized particles with enzymes. We can better understand the enhancement as a function of particle size by considering how particle size and the observed enhancements in diffusion relate to one another.

To ensure breaking down the symmetry of the enzyme molecules distribution on the surface of the particles, we attend to use half gold-coated particles, which allows coating only one side of the surface of the particles with enzymes resulting in nonuniformly distributed enzymes on the particles.

In summary, we have established a methodology to carry out a conclusive test of enhanced diffusion of enzymes.

Chapter 5

Appendices

5.1 Step-by-Step Guide to AP-Nanoparticle Synthesis

5.1.1 Preparing The Solutions

- **Vial A**, 16.6 mg/ml of 200 nm amine functionalized polystyrene spherical particles, dispersed in water from Millipore Sigma, in Dulbecco's phosphate-buffered saline (DPBS), purchased from Millipore Sigma, prepared as the following:

    1. Add 1 ml of (275 - 304) mOsm/kg DPBS to 0.5 ml of 25 mg/ml amine functionalized polystyrene particles (diameter = 200 nm) in water.
    2. Centrifuge for 8 minutes at 150000 RPM, 20353×g, 10°C. Then, concentrate to 0.75 ml, add 1 ml of DPBS and mix gently by hand until the particles are well dispersed.
    3. Repeating step 2 two more times gives 1.75 ml of 7.14 mg/ml of amine-functionalized polystyrene particles dispersed in DPBS.
    4. Applying ultrasound waves using the ultrasonic bath BRANSON 8510 on the sample for 10 minutes at temperature 24°C will get rid of any aggregation after centrifuging and redispersing multiple times in the previous steps.

- **Vial B**, 18% glutaraldehyde in DPBS.
- **Vial C**, 0.43 ml of alkaline phosphatase 1.84 mg/ml, 13.14 mM (12.5 kU/ml) in DPBS.
- **Vial D**, 0.2 M ethanolamine in DPBS.
- **Vial E**, 1 mg/ml of bovine serum albumin (BSA) lyophilized powder, purchased from Millipore Sigma, was dissolved in DPBS.
- **Vial F**, tris_HCl 0.1M, pH 7.6 buffer.

5.1.2 The Procedure

1. Mix 0.75 ml of **vial B** with 1 ml of **vial A** on a tube rotator at 30 RPM at room temperature for 6 hours to attach the glutaraldehyde molecules with the amino group on the surface of the particles.
2. Centrifuge for 5 minutes at 150000 RPM, 20353×g, 10°C, then concentrate to 0.25 ml, add 1 ml of DPBS and mix until the particles are fully dispersed.
3. Repeat step 2 two more times.
4. Centrifuge again same as for step 2, but this time remove all the supernatants. Then, re-disperse the particles in DPBS until the total volume is 1.25 ml.
5. Apply ultrasound waves using the ultrasonic bath BRANSON 8510 for 3 minutes at temperature 24°C.
6. Add **Vial C** to the solution and mix on a tube rotator at 30 RPM at room temperature for 18 hours of occupation time in order to attach enzyme molecules to the glutaraldehyde on the surface of the particles.
7. Centrifuge for 5 minutes at 150000 RPM, 20353×g, 10°C and remove all the supernate, then re-disperse in DPBS until the total volume is 1 ml.
8. Add 1 ml of **Vial D** and mix on the tube rotator at 30 RPM for 30 minutes. This step serves to block unreacted sites on the particles.
9. centrifuge for 5 minutes at 150000 RPM, 20353×g, 10°C and concentrate the sample to 0.75 ml.
10. Add 0.75 ml of **Vial E**.
11. Centrifuge for 5 minutes at 150000 RPM, 20353×g, 10°C and remove all the supernate.
12. Add **Vial E** until the total volume is 1.25 ml. The BSA should block any remaining polymer particle surfaces and minimize nonspecific protein binding in downstream assays.
13. Centrifuge for 5 minutes at 150000 RPM, 20353×g, 10°C and concentrate to 0.75 ml. Then, add 0.75 ml of **Vial F**.
14. Repeat step 13 two more times.
15. Centrifuge again same for as step 13 but remove all supernate this time and re-disperse in **Vial F** until the total volume is 1 ml.
16. Extra washes by repeating step 15 three times were done (supernatant was saved for free enzymes test in 4.2.1).

The final sample is 1 ml of 7.14 mg/ml of 200nm AP(alkaline phosphates)-nP(nanoparticles) in Tris_HCl 0.1 M, pH 7.6 stored at 4°C.

Bibliography

[1] Hari S. Muddana, Samudra Sengupta, Thomas E. Mallouk, Ayusman Sen, and Peter J. Butler. Substrate catalysis enhances single-enzyme diffusion. *Journal of the American Chemical Society*, 132:2110–2111, 2 2010.

[2] Tania Patiño, Natalia Feiner-Gracia, Xavier Arqué, Albert Miguel-López, Anita Jannasch, Tom Stumpp, Erik Schäffer, Lorenzo Albertazzi, and Samuel Sánchez. Influence of enzyme quantity and distribution on the self-propulsion of non-janus urease-powered micromotors. *Journal of the American Chemical Society*, 140:7896–7903, 6 2018.

[3] Leonor Michaelis and Maud L Menten. Die kinetik der invertinwirkung biochem z 49: 333–369. *Find this article online*, 1913.

[4] Roberto Cerbino and Veronique Trappe. Differential dynamic microscopy: Probing wave vector dependent dynamics with a microscope. *Phys. Rev. Lett.*, 100:188102, May 2008.

[5] Mathieu Leocmach. Ddm python 2. *https://github.com/MathieuLeocmach/DDM/*, 2015.

[6] H. Bisswanger. *Enzyme Kinetics: Principles and Methods*. Wiley, 2017.

[7] Eunice E. Kim and Harold W. Wyckoff. Reaction mechanism of alkaline phosphatase based on crystal structures. *Journal of Molecular Biology*, 218:449–464, 3 1991.

[8] Polysciences Inc. Glutaraldehyde coupling kit with hollow fiber filtering system. *Journal of Molecular Biology*, 2011.

[9] Brown R. A brief account of microscopical observations on the particles contained in the pollen of plants and the general existence of active molecules in organic and inorganic bodies. *Edinburgh New Philosophical Journal*, pages 358–371, 1827.

[10] A. Einstein. Über die von der molekularkinetischen theorie der wärme geforderte bewegung von in ruhenden flüssigkeiten suspendierten teilchen. *Annalen der Physik*, 322:549–560, 1905.

[11] A. Meller, R. Bar-Ziv, T. Tlusty, E. Moses, J. Stavans, and S.A. Safran. Localized dynamic light scattering: A new approach to dynamic measurements in optical microscopy. *Biophysical Journal*, 74(3):1541–1548, 1998.

[12] Bernard Lorber, Frédéric Fischer, Marc Bailly, Hervé Roy, and Daniel Kern. Protein analysis by dynamic light scattering: Methods and techniques for students. *Biochemistry and Molecular Biology Education*, 40(6):372–382, 2012.

[13] Joseph W Goodman. Introduction to fourier optics. *Introduction to Fourier optics, 3rd ed., by JW Goodman. Englewood, CO: Roberts & Co. Publishers, 2005*, 1, 2005.

[14] H Köhler. On abbe's theory of image formation in the microscope. *Optica Acta: International Journal of Optics*, 28(12):1691–1701, 1981.

[15] Ronald Newbold Bracewell and Ronald N Bracewell. *The Fourier transform and its applications*, volume 31999. McGraw-Hill New York, 1986.

[16] Bruce J Berne and Robert Pecora. *Dynamic light scattering: with applications to chemistry, biology, and physics*. Courier Corporation, 2000.

[17] K.J. Denniston, J.J. Topping, and R.L. Caret. *General, Organic, and Biochemistry*. McGraw-Hill Higher Education, 2003.

[18] P. J. Butterworth. Fundamentals of enzyme kinetics (3rd edn) a. cornish-bowden. portland press ltd, london, 422+xvi pp., isbn 1 85578 158 1 (2000). *Cell Biochemistry and Function*, 23(4):292–292, 2005.

[19] Victor Henri. Théorie générale de l'action de quelques diastases par victor henri [cr acad. sci. paris 135 (1902) 916-919]. *Comptes rendus. Biologies*, 329(1):47–50, 2006.

[20] George Edward Briggs and John Burdon Sanderson Haldane. A Note on the Kinetics of Enzyme Action. *Biochemical Journal*, 19(2):338–339, 01 1925.

[21] Hans Lineweaver and Dean Burk. The determination of enzyme dissociation constants. *Journal of the American Chemical Society*, 56:658–666, 3 1934.

[22] Samuel Sánchez and Martin Pumera. Nanorobots: the ultimate wireless self-propelled sensing and actuating devices. *Chemistry, an Asian journal*, 4:1402–10, 9 2009.

[23] Joseph Wang. Can man-made nanomachines compete with nature biomotors? *ACS nano*, 3:4–9, 1 2009.

[24] Samudra Sengupta, Krishna K. Dey, Hari S. Muddana, Tristan Tabouillot, Michael E. Ibele, Peter J. Butler, and Ayusman Sen. Enzyme molecules as nanomotors. *Journal of the American Chemical Society*, 135:1406–1414, 1 2013.

[25] Clement Riedel, Ronen Gabizon, Christian A. M. Wilson, Kambiz Hamadani, Konstantinos Tsekouras, Susan Marqusee, Steve Pressé, and Carlos Bustamante. The heat released during catalytic turnover enhances the diffusion of an enzyme. *Nature*, 517:227–230, 1 2015.

[26] Pierre Illien, Xi Zhao, Krishna K. Dey, Peter J. Butler, Ayusman Sen, and Ramin Golestanian. Exothermicity is not a necessary condition for enhanced diffusion of enzymes. *Nano Letters*, 17:4415–4420, 7 2017.

[27] Michael Börsch, Paola Turina, Christian Eggeling, Joachim R Fries, Claus A.M Seidel, Andreas Labahn, and Peter Gräber. Conformational changes of the h+-atpase from escherichia coli upon nucleotide binding detected by single molecule fluorescence. *FEBS Letters*, 437:251–254, 10 1998.

[28] Jan-Philipp Günther, Michael Börsch, and Peer Fischer. Diffusion measurements of swimming enzymes with fluorescence correlation spectroscopy. *Accounts of Chemical Research*, 51:1911–1920, 9 2018.

[29] Jan-Philipp Günther, Günter Majer, and Peer Fischer. Absolute diffusion measurements of active enzyme solutions by nmr. *The Journal of Chemical Physics*, 150:124201, 3 2019.

[30] Krishna K. Dey, Xi Zhao, Benjamin M. Tansi, Wilfredo J. Méndez-Ortiz, Ubaldo M. Córdova-Figueroa, Ramin Golestanian, and Ayusman Sen. Micromotors powered by enzyme catalysis. *Nano Letters*, 15:8311–8315, 12 2015.

[31] Xing Ma, Xu Wang, Kersten Hahn, and Samuel Sánchez. Motion control of urea-powered biocompatible hollow microcapsules. *ACS Nano*, 10:3597–3605, 3 2016.

[32] Ana C. Hortelão, Tania Patiño, Ariadna Perez-Jiménez, Àngel Blanco, and Samuel Sánchez. Enzyme-powered nanobots enhance anticancer drug delivery. *Advanced Functional Materials*, 28:1705086, 6 2018.

[33] Zhijie Chen, Alan Shaw, Hugh Wilson, Maxime Woringer, Xavier Darzacq, Susan Marqusee, Quan Wang, and Carlos Bustamante. Single-molecule diffusometry reveals no catalysis-induced diffusion enhancement of alkaline phosphatase as proposed by fcs experiments. *Proceedings of the National Academy of Sciences*, 117:21328–21335, 9 2020.

[34] Douglas Magde, Elliot Elson, and W. W. Webb. Thermodynamic fluctuations in a reacting system—measurement by fluorescence correlation spectroscopy. *Physical Review Letters*, 29:705–708, 9 1972.

[35] William S. Price. Pulsed-field gradient nuclear magnetic resonance as a tool for studying translational diffusion: Part ii. experimental aspects. *Concepts in Magnetic Resonance*, 10:197–237, 1998.

[36] D. Axelrod, D.E. Koppel, J. Schlessinger, E. Elson, and W.W. Webb. Mobility measurement by analysis of fluorescence photobleaching recovery kinetics. *Biophysical Journal*, 16:1055–1069, 9 1976.

[37] Juan Yguerabide and Evangelina E. Yguerabide. Light-scattering submicroscopic particles as highly fluorescent analogs and their use as tracer labels in clinical and biological applications: I. theory. *Analytical Biochemistry*, 262(2):137–156, 1998.

[38] Yukikazu Uemura, Mineo Fujimura, Takeji Hashimoto, and Hiromichi Kawai. Application of light scattering from dielectric cylinder based upon mie and rayleigh—gans—born theories to polymer systems. i. scattering from a glass fiber. *Polymer Journal*, 10:341–351, 1978.

[39] Harnoor Singh. Ddm python 3. *https://github.com/harnoor-singh/DDM-util*, 2022.

[40] Rob L. Dean. Kinetic studies with alkaline phosphatase in the presence and absence of inhibitors and divalent cations. *Biochemistry and Molecular Biology Education*, 30:401–407, 11 2002.